Peer-reviewed version available at Sustainability 2018, 10, 2503; doi:10.3390/su10072503

Type of the Paper (Article)

Properties of Fired Bricks by Incorporating TFT-LCD Waste Glass Powder with Reservoir Sediments

Chao-Wei Tang [1,*]

[1] Department of Civil Engineering & Geomatics, Cheng Shiu University, No. 840, Chengcing Rd., Niaosong District, Kaohsiung 83347, Taiwan
* Correspondence: tangcw@gcloud.csu.edu.tw; Tel.: +886-7-735-8800

Abstract: In view of increasing concerns over non-renewable resource depletion and waste management, this study aimed to apply the Taguchi optimization technique to determine the process conditions for producing bricks by incorporating thin film transition liquid crystal displays (TFT-LCD) waste glass powder with reservoir sediments. An orthogonal array $L_{16}(4^5)$ was adopted, which consisted of five controllable four-level factors (i.e., cullet content, drying method, preheat time, sintering temperature, and error). Moreover, the analysis of variance method was used to explore the effects of the experimental factors on the density, water absorption, shrinkage ratio, loss of ignition, porosity, and compressive strength of the fired bricks. The microstructures of the fired specimens were investigated by scanning electron microscopy. Then, the large-scale production techniques for fired bricks containing recycled TFT-LCD glass cullet and reservoir sediments was developed in a commercially available tunnel kiln. The test results showed that the structure of fired specimen was loose at a sintering temperature ranged from 900–950 °C. However, the fired specimen showed a significant densification at the sintering temperature of 1050 °C. In addition, Taguchi method is a feasible approach for optimizing process condition of brick using recycled TFT-LCD glass cullet and reservoir sediments and it significantly reduces the number of tests. On the other hand, the characteristics of fired bricks developed in the tunnel kiln were in compliance with Chinese National Standards class I building bricks criteria.

Keywords: reservoir sediments; cullet; brick; sintering; orthogonal array

1. Introduction

Bricks are mainly made from clay by burning it at high temperatures [1]. The manufacture of bricks can be traced back to centuries CE. As early as 2000 BC, a large brick kiln was excavated in Gujarat, India [1,2]. The use of clay in China to manufacture bricks and tiles as a building material began in the Qin and Han dynasties and has a history of more than 2,200 years [1]. Therefore, it has always been the most commonly used building material in mainland China. As for the bricks and tiles used in Taiwan, they were first introduced by Chinese immigrants. It was not until the Dutch occupied Taiwan in the 1620s that they started making bricks, and during the period of Zheng Chenggang's rule in the 1660s, it began to manufacture tiles. From the above, it can be seen that the development of bricks and tiles in Taiwan has a history of more than 400 years.

With their attractive appearances and superior properties such as high compressive strength and durability, excellent fire and weather resistance, good thermal and sound insulation, bricks have long been widely used in building, civil engineering work, and landscape design [3]. The main raw materials of clay bricks are natural resources such as clay or shale, but with the concept of sustainable development and the raising awareness of environmental protection, the exploitation or acquisition of these raw materials has become increasingly difficult in Taiwan. There have been many related studies concerning the development of alternative sources of clay bricks [4-24]. These alternative

materials include: surplus soil for construction projects, reservoir sediments, water purification sludge, slag, inorganic sludge, stone waste, fly ash, palm oil fuel ash, incinerator ash and waste glass, etc. Among them, many studies report the use of glass as a brick fluxing agent.

Harrison [4] added cullet to two types of clay, one as a buff clay and the other as a red clay, with percentages of substitution of 0, 5, and 10% to explore its feasibility for brick making and to evaluate the actual mass production process. The results of laboratory-scale trial firing showed that at the same sintering temperature, the water absorption of the brick decreased with the increase of the amount of cullet, while the compressive strength of the brick increased with the addition of cullet. In addition, regardless of the type of clay, the color of the brick became darker as the added amount of cullet increases. Smith [6] also used cullet to blend in clay, with substitution percentages of 0, 5, and 10%, respectively, to assess the feasibility of the actual mass production process. The results of the firing indicated that at the same sintering temperature, the water absorption rate of bricks after immersing in cold water for 24 hours decreased with the increase of the amount of cullet, while the compressive strength of bricks increased with the increase of the amount of cullet. However, in the experimental group, the water absorption and compressive strength of the brick blended with 5% cullet were similar to those of the 10%, and there was no significant difference. Moreover, regardless of the sintering temperature of 950 or 970 °C, the bricks presented a pristine appearance, and the color difference between the control group and the experimental group was not significant. Rahman *et al.* [7] investigated the performance of brick where cement is replaced by fly ash and palm oil fuel ash. Their test results revealed that both fly ash and palm oil fuel ash incorporated bricks satisfied Class 1 and Class 2 load-bearing brick requirements according to the Malaysian Standard MS76:1972 along with water absorption requirements as per ASTM C55-11. Muntohar and Rahman [9] presented an experimental study on the development of the shellcrete masonry block that made of oil palm kernel. Their test results revealed that the greater oil palm kernel content tend to have a lower density and absorbed water easily. Ean *et al.* [10] investigated the effects of pre-wetted unit bricks, mortar type and slenderness ratio of prisms on the compressive strength and failure mode of sediment brick. Their test results showed that pre-wetted sediment brick masonry exhibited higher compressive strength of up to 20% compared to the dry sediment masonry. Especially, using cement-lime mortar led to lower compressive strength compared to cement mortar. However, the sediment brick masonry with the cement lime mortar exhibited higher compressive strength in comparison with cement mortar masonry. On the other hand, in terms of production technology, the industry has gradually emphasized clean production or research and development of burn-free processes to reduce energy consumption. According to Kirby's results [11], the energy used to produce cullet/clay bricks (natural gas) was 38.9% less than that of clinker/clay bricks.

In the thin film transition liquid crystal displays (TFT-LCD) manufacturing industry, Taiwan is the leading country. According to statistics from the Department of Waste Management under the Taiwan Environmental Protection Administration (EPA) in July 2008, the amount of used TFT-LCD glass produced in Taiwan had grown very rapidly. Therefore, it is necessary to actively promote new recycling applications of TFT-LCD waste glass in Taiwan. Basically, TFT-LCD waste glass can be divided into three major types: waste glass, waste coated glass, and waste black glass. Among them, waste glass is an uncoated glass that has not been injected with liquid crystal and can be sent to a recycling organization for recycling and reuse; waste coated glass is a glass plate with a color filter or a transparent conductive layer or alignment film; and waste black glass is a kind of coated glass with polarizer attached. The main source of waste glass is the edge material, scrap or defective product produced during the manufacture of liquid crystal panels. However, the current research on incorporating TFT-LCD waste glass with reservoir sediments to produce bricks is extremely rare.

In general, the factors affecting the performance of fired bricks include raw materials composition and firing conditions [1-7,22]. In a factorial design, as the design parameters or parameter levels increase, not only the time and cost of the experiment increase significantly, but the experimental conditions become more complicated. In contrast, the Taguchi method only tests pairs of combinations instead of having to test all possible combinations [25–28]. This is mainly due to the fact that Taguchi's orthogonal arrays are highly fractional orthogonal designs [25]. In particular, these

designs can use only the minimum number of experiments to estimate the main effects, thereby saving time and resources [25-28]. As a result, Taguchi method can effectively improve the quality of products, and has the advantages of economy, operability, and robustness.

In view of the above considerations, the present study aimed at conducting an investigation on the development of bricks by incorporating TFT-LCD waste glass with reservoir sediments. The experiments were designed using an orthogonal array technique in an L_{16} array with four controllable four-level factors. Moreover, the large-scale production techniques for producing clay bricks containing recycled TFT-LCD glass cullet was developed in a commercially available tunnel kiln.

2. Experimental Details

2.1. Materials and Test Items

In this study, the main materials used included grinding TFT-LCD glass and reservoir sediments. The TFT-LCD waste glass was used as an additive, and it was blended with reservoir sediments to burn building bricks. The grinding TFT-LCD glass was collected from a panel factory in Taichung, Central Taiwan. The reservoir sediments were collected from the Wushoh Reservoir located in Central Taiwan. Each raw material sample was collected first, and the mineral composition, physical properties, and chemical composition tests were performed to confirm that the composition and basic properties were in line with the raw material requirements for burning high-quality clay bricks. For reservoir sediments, X-ray powder diffraction analysis was used. The intensity of the spectral analysis was used to compare the maps of the standard samples and the mineralogical composition was quantitatively analyzed according to the standard mineralogy algorithm based on the material chemical composition. Physical property analysis of raw materials included specific gravity, moisture content, particle size analysis, and plasticity (liquid limit, plastic limit, and plasticity index). Chemical analysis of raw materials was based on quantitative analysis of X-ray fluorescence. The result of any test was the average of three specimens, to ensure the reliability of the results.

2.2. Experimental Program

The Taguchi method was adopted to design the experimental protocol. Cullet content, drying method, preheat time, sintering temperature, and error were selected as the process parameters. The fifth factor is for error calculation. The levels of these parameters are given in Table 1. In addition, Table 1 also shows that density, water absorption, shrinkage ratio, loss on ignition, porosity, and compressive strength of the resulting brick were used as the performance parameters for this research. Moreover, an orthogonal array $L_{16}(4^5)$ was adopted, which consisted of five controllable four-level factors (Table 2). The last column of the orthogonal array is left empty for the error detection of experiments.

Table 1. Process parameters and design levels.

Parameter (Experimental Control Factor)	Levels of Parameter				Performance Parameter
	1	2	3	4	
Cullet Content, A (%)	0	10	20	30	Density (g/cm^3)
Drying Method, B	DM1	DM2	DM3	DM4	Water Absorption (%)
Preheat Time, C (min)	60	90	120	150	Shrinkage Ratio (%)
Sintering Temperature, D (°C)	900	950	1000	1050	Loss on Ignition (%)
Error, E	-	-	-	-	Porosity (%)
					Compressive Strength (kgf/cm^2)

The effects of the composition and firing conditions on the properties of the resulting brick were evaluated with a laboratory-scale setup. On the other hand, the range analysis and analysis of variance (ANOVA) were the mathematical statistics used to explore the effects of the experimental factors on the performances of the produced bricks, thus optimizing the selected parameters.

Table 2. Orthogonal array for $L_{16}(4^5)$.

Experiment Number	Parameter (Level)				
	A	B	C	D	E
G1	0(1)*	DM1(1)	60(1)	900(1)	—(1)
G2	0(1)	DM2(2)	90(2)	950(2)	—(2)
G3	0(1)	DM3(3)	120(3)	1000(3)	—(3)
G4	0(1)	DM4(4)	150(4)	1050(4)	—(4)
G5	10(2)	DM1 (1)	90(2)	1000(3)	—(4)
G6	10(2)	DM2 (2)	60(1)	1050(4)	—(3)
G7	10(2)	DM3 (3)	150(4)	900(1)	—(2)
G8	10(2)	DM4 (4)	120(3)	950(2)	—(1)
G9	20(3)	DM1 (1)	120(3)	1050(4)	—(2)
G10	20(3)	DM2 (2)	150(4)	1000(3)	—(1)
G11	20(3)	DM3 (3)	60(1)	950(2)	—(4)
G12	20(3)	DM4 (4)	90(2)	900(1)	—(3)
G13	30(4)	DM1 (1)	150(4)	950(2)	—(3)
G14	30(4)	DM2 (2)	120(3)	900(1)	—(4)
G15	30(4)	DM3 (3)	90(2)	1050(4)	—(1)
G16	30(4)	DM4 (4)	60(1)	1000(3)	—(2)

Note: * The numbers in parentheses indicate the level of the factor.

2.3. Laboratory-scale Firing Test

In order to avoid the phenomenon that certain ingredients of raw materials are too concentrated and cause unreasonable results, samples of the raw materials need to be subjected to aging treatment. To facilitate the brick making process and achieve better firing results, the TFT-LCD waste glass and reservoir sediments were first crushed, and then refinement processes such as crushing and ball milling were applied to ensure homogenization of the raw materials (Figure 1).

(a) (b) (c) (d)

Figure 1. Raw materials. (a) Original TFT-LCD waste glass; (b) Refined TFT-LCD glass powder; (c) Original reservoir sediments; (d) Refined reservoir sediments.

Figure 2(a) shows the resulting fine powders were thoroughly mixed to ensure homogeneity as per the design ratio in Table 2. Subsequently, an appropriate amount of water (18% by weight mixture) was added to the mixture, as shown in Figure 2(b). It is important to moisten each clay particle surface to increase clay plasticity. In addition, through the rubbing process, the air in the mixture was squeezed out, and in the course of the process, the uneven masses were combined and kneaded again to obtain a smooth and well-proportioned embryo, as shown in Figure 2(c). Place the plastic mixture after soil training into a test brick model with a length of 50 mm, a width of 50 mm, and a height of 50 mm, as shown in Figure 3(a). Then a small universal compressive tester was used to apply an appropriate pressure to press the plastic mixture in each brick mold to form a brick embryo, as shown in Figure 3(b). There was a total of 16 groups of brick embryos (G1-G16) with 3 trials in each group, as shown in Figure 3(c). It must be noted that the shaped brick embryo must possess sufficient tensile strength to maintain its shape.

Preprints (www.preprints.org) | NOT PEER-REVIEWED | Posted: 14 June 2018 doi:10.20944/preprints201806.0229.v1

Peer-reviewed version available at Sustainability 2018, 10, 2503; doi:10.3390/su10072503

(a) (b) (c)

Figure 2. Raw material mix. (a) Dry mix; (b) Water mixing; (c) Well-proportioned embryo.

(a) (b) (c)

Figure 3. Brick forming. (a) Placing plastic material in brick mold; (b) Applying load; (c) Brick embryos.

After the formation of the "green" brick embryo, the moisture content will cause the brick embryo to shrink during the drying process, which has a great influence on the quality of the finished product. Therefore, the brick embryo must be dried. According to the design of the orthogonal table in Table 1, the brick embryos were applied to four different drying methods (DM1: natural drying for 2 days (dry at room temperature); DM2: natural drying for 1 day (dry at room temperature); DM3: oven drying for 1 day (operating temperature 100 °C); and DM4: oven drying for 1 day (operating temperature 50 °C).

After treatment with different drying methods, the moisture content of the 16 groups of brick embryos is shown in Table 3. From the table, it can be seen that the moisture content of brick embryos after “natural drying for 1 day” was the largest, ranging from approximately 14.2% to 14.9%, and the moisture content of brick embryos after “natural drying for 2 days” was the next, approximately between 10.3% and 11.6%. The brick embryos dried at “50 °C for 1 day” were about 1.1-3.3%. The moisture content of the brick embryos that were “dried at 100 °C for 1 day” was the smallest, and the moisture content was 0%.

Table 3. Moisture content of brick embryos.

Experiment Number	Drying Method	Moisture Content of Green Brick Embryos (%)	Moisture Content of Dry Brick Embryos (%)
G1	DM1	18.0	11.6
G5		18.0	11.1
G9		18.0	10.3
G13		18.0	10.4
G2	DM2	18.0	14.9
G6		18.0	14.8
G10		18.0	14.2
G14		18.0	14.3
G3	DM3	18.0	0.0
G7		18.0	0.0
G11		18.0	0.0
G15		18.0	0.0
G4	DM4	18.0	1.1
G8		18.0	1.6
G12		18.0	2.4
G16		18.0	3.3

After the brick embryos was dried, they were placed in an alumina crucible and placed in a programmable high temperature electric furnace, as shown in Figure 4. Then, the temperature of the

furnace was heated from room temperature to 500 °C. The preheating time is shown in Table 1. The preheating process can not only make the brick embryos had a certain strength, but also can avoid the bursting phenomenon during the firing process. Once the brick embryos had completed the preheating process, they were immediately placed in another high-temperature electric furnace that had been set at the sintering temperature for the firing operation. The sintering temperature used is shown in Table 1, while the sintering time was kept constant. When the brick embryos had finished the firing process, they were slowly cooled (in-furnace cooling). When the temperature of the bricks fell to room temperature, their physical and mechanical properties were measured.

Figure 4. High-temperature electric furnaces (for baking on the left and for preheating on the right).

2.4. Test Methods and Data Analysis

As previously described, the characteristics of the resulting bricks were evaluated by six performance parameters (brick density, water absorption, shrinkage ratio, loss of ignition, porosity, and compressive strength). The density of the sintered bricks is determined by the Archimedes principle, as shown below:

$$\rho = \frac{m_{dry}}{m_{sat} - m_{imm}} \quad (1)$$

where ρ= brick density (g/cm^3); m_{dry} = dry mass (g/cm^3); m_{imm} = immersed mass (g/cm^3); and m_{sat} = 24-h saturated surface-dry mass (g/cm^3).

The water absorption was determined by dipping the sintered bricks in water for 24 h, and oven dried subsequent to immersion at 115 °C for not less than 24 h. The amount of absorbed water was calculated by the following formula:

$$\text{Water absorption } (W_a) = \frac{m_{sat} - m_{dry}}{m_{dry}} \times 100\% \quad (2)$$

To explore the volume change of the brick embryos, the size of the embryos before and after sintering was measured. The shrinkage ratio was defined as the ratio of the volume of the fired embryo to the volume of the unfired embryo, which was calculated as follows:

$$\text{Shrinkage ratio } (S_r) = \frac{V_g - V_s}{V_g} \times 100\% \quad (3)$$

where V_g = initial volume of the green brick embryo; and V_s = volume of the sintered brick embryo.

Loss on ignition was defined as the mass loss of the dried brick embryo after firing and was expressed as a percentage of the total initial mass. Compressive strength is usually defined as the failure stress measured normal to the bed face of the brick. The compressive strength test was performed in the dry specimens. The test method referred to the standard test of ASTM C67 [29].

The signal-to-noise ratio (*S*/*N* ratio) for each control factor can be used to evaluate the effect of each selected factor on the quality characteristics being studied [25]. The *S*/*N* ratio is calculated by the mean squared deviation (*MSD*) [30]. In fact, the purpose of any experiment is to determine the highest possible *S*/*N* ratio for the result. If the *S*/*N* ratio (η) for the-smaller-the-better target for all the responses is expressed in decibels (dB), it can be defined by a logarithm based on the *MSD* around the target value, as shown below [30]:

Peer-reviewed version available at Sustainability 2018, 10, 2503; doi:10.3390/su10072503

$$\eta = -10 \times \log_{10}(MSD) = -10 \times \log_{10}\left(\frac{1}{n}\sum_{i=1}^{n} y_i^2\right) \quad (4)$$

where n is the number of repetitions or observations; and y_i is the observed data. In the case of the-larger-the-better target, the S/N ratio (η) is generally derived from the reciprocal of its quality characteristics value, as shown below [30]:

$$\eta = -10 \times \log_{10}(MSD) = -10 \times \log_{10}\left(\frac{1}{n}\sum_{i=1}^{n} \frac{1}{y_i^2}\right) \quad (5)$$

In this study, the observed values of brick density, water absorption, shrinkage ratio, loss of ignition, and porosity were set to a minimum level, while the observed values of the compressive strength were set to a maximum level. Moreover, the analysis of variance (ANOVA) was used to detect the optimization of the observed values. This was accomplished by separating the total variability of the S/N ratios into contributions by each of the process parameters and the error [31].

3. Results and Discussion

3.1. Physical Properties and Chemical Composition Analysis of Raw Materials

In the case of raw materials for making bricks, the finer the particle size, the better. Due to the greater dispersion and better uniformity of the finely divided raw materials, there is a relatively large contact area between the particles, which allows them to have good thermal efficiency and firing results at high temperatures. Furthermore, in addition to the easy mixing of raw materials having a fine particle size, the strength of the produced brick embryos is high, and the fired bricks have a relatively better compressive strength. In general, making high-strength bricks requires that the particle size of the powdery materials should be less than 150 μm.

The particle size distribution characteristics for the grinding cullet and reservoir sediments are shown in Figure 5. According to Figure 5, the diameter of the milled glass was larger, and its average particle diameter was 357 μm, which means that the glass should be ground again to facilitate the batching or firing; the particle size of the reservoir sediments was fine, and the average particle size was 30.34 μm. From this, although the glass had been ground and refined, its particle size was still large. In order to make the ingredients even and make high-strength bricks, the glass was sieved with a No. 100 sieve (<150 μm), and the glass passed through the sieves was used as a test material.

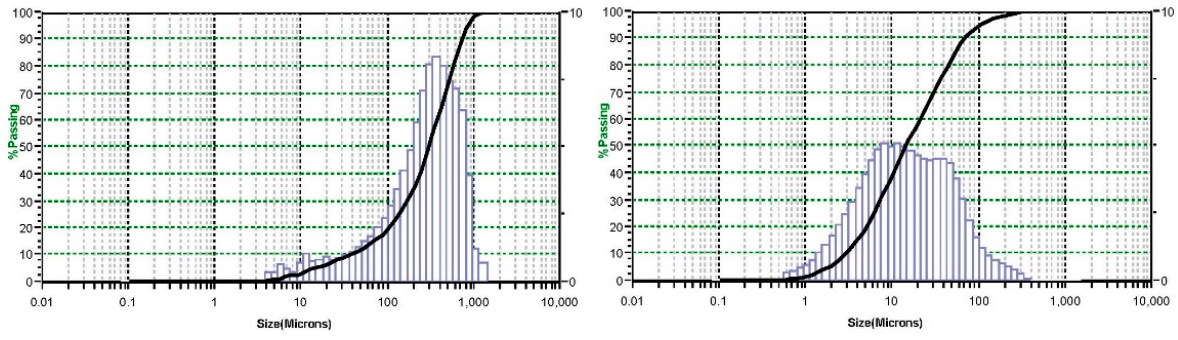

(a) (b)

Figure 5. Grain size distributions of TFT-LCD waste glass and reservoir sediments. (a) Refined TFT-LCD glass powder; (b) Refined reservoir sediment.

Basically, the plasticity of raw materials has a great influence on the production of brick embryos. In general, the plasticity index (PI) of raw materials should be between 12-16. Table 4 shows that the plasticity of the glass was poor (no plasticity); the plasticity of the reservoir sediments (PI=14) is better, which can meet the requirements for the production of brick embryos. For the specific gravity analysis of raw materials, the specific gravity of the reservoir sediments was about 2.49, which

was similar to the specific gravity of the general soil, while the specific gravity of the glass was relatively small, about 2.3.

Table 4. Analytical results of physical properties of raw materials.

Sample type	Specific Gravity	Plasticity Index (P.I.)	Average Particle size (μm)	Maximum Particle Size (μm)	Minimum Particle Size (μm)
Reservoir Sediments	2.49	14	30.34	418.6	0.688
TFT-LCD Waste Glass	2.3	N.P.	357	1,408	4.62

The chemical composition of sediments and glass is shown in Table 5. Loss on ignition (LOI) at 450°C, reservoir sediments was 3.9%; glass had almost no ignition loss (0.04%), indicating that the organic content of the raw material was low. As can be seen from Table 5, the main chemical components of these two materials are approximately SiO_2 and Al_2O_3, which account for 82% and 91% of the components, respectively. In addition, the main difference between the two is that the Al_2O_3 content of the reservoir sediments (23.8%) was higher, and the SiO_2 content of the glass (85.4%) was significantly higher.

Table 5. Chemical composition of sludge and reservoir sediments.

Sample	Chemical Compositions (wt %)									
	SiO_2	Al_2O_3	Fe_2O_3	CaO	MgO	K_2O	Na_2O	OS	LOI	Total
Reservoir Sediments	58.4	23.8	5.9	3.6	2.6	4.2	1.5	-	3.9	100
TFT-LCD Waste Glass	85.4	5.6	0.2	-	2.5	-	6.3	-	0.04	100

Notes: LOI = loss on ignition; OS = organic substance content.

3.2. Density

Table 6 shows the experimental results and the corresponding *S/N* ratios using Equations (4) or (5). In addition, the photographs of the bricks fired in each group are shown in Figure 6. As the experimental design was orthogonal, the effect of each parameter used could be separated at different levels. Taking the cullet content as an example, the mean *S/N* ratio at levels 1, 2, 3, and 4 were calculated by averaging the *S/N* ratios of experiments 1–4, 5–8, 9–12, and 13–16, respectively. As for the other parameters, the mean *S/N* ratio at each level was computed in a similar manner. The influence of each selected factor on the quality characteristic investigated is described in detail below.

Table 6. Experimental results and *S/N* ratio.

Experiment Number	Experimental Results						*S/N* Ratio (dB)					
	ρ (g/cm³)	W_a (%)	S_r (%)	LOI (%)	V_V (%)	f_c' (MPa)	ρ	W_a	S_r	LOI	V_V	f_c'
G1	1.67	29.0	34.4	17.4	42.7	3.31	-4.45	-29.25	-30.73	-24.81	-32.61	10.40
G2	1.60	27.4	22.9	20.6	40.5	4.03	-4.08	-28.76	-27.20	-26.28	-32.15	12.11
G3	1.66	18.9	28.3	5.6	28.4	6.93	-4.40	-25.53	-29.04	-14.96	-29.07	16.81
G4	1.57	30.3	22.2	7.6	44.1	5.05	-3.92	-29.63	-26.93	-17.62	-32.89	14.07
G5	1.84	18.5	47.6	16.3	28.6	9.50	-5.30	-25.34	-33.55	-24.24	-29.13	19.55
G6	1.68	21.0	25.1	19.9	32.2	12.09	-4.51	-26.44	-27.99	-25.98	-30.16	21.65
G7	1.61	25.0	12.5	5.4	38.6	3.34	-4.14	-27.96	-21.94	-14.65	-31.73	10.47
G8	1.68	18.6	23.1	7.5	28.8	7.38	-4.51	-25.39	-27.27	-17.50	-29.19	17.36
G9	1.67	25.8	24.9	14.7	39.5	14.11	-4.45	-28.23	-27.92	-23.35	-31.93	22.99
G10	1.74	19.2	21.1	18.5	31.1	11.05	-4.81	-25.67	-26.49	-25.34	-29.86	20.87
G11	1.69	20.4	22.0	4.7	32.0	5.95	-4.56	-26.19	-26.85	-13.44	-30.10	15.49
G12	1.73	18.5	23.8	7.0	29.5	4.19	-4.76	-25.34	-27.53	-16.90	-29.40	12.44
G13	1.84	12.5	37.0	14.4	20.1	6.05	-5.30	-21.94	-31.36	-23.17	-26.06	15.64
G14	1.72	18.8	21.7	17.8	30.0	3.78	-4.71	-25.48	-26.73	-25.01	-29.54	11.55
G15	1.72	17.7	19.1	4.1	28.4	14.70	-4.71	-24.96	-25.62	-12.26	-29.07	23.35
G16	1.77	13.7	31.2	7.6	21.7	10.49	-4.96	-22.73	-29.88	-17.62	-26.73	20.42

Note: ρ = density; W_a = water absorption; S_r = shrinkage ratio; LOI = loss on ignition; V_V = porosity; and f_c'= compressive strength.

Preprints (www.preprints.org) | NOT PEER-REVIEWED | Posted: 14 June 2018 doi:10.20944/preprints201806.0229.v1

Peer-reviewed version available at Sustainability 2018, 10, 2503; doi:10.3390/su10072503

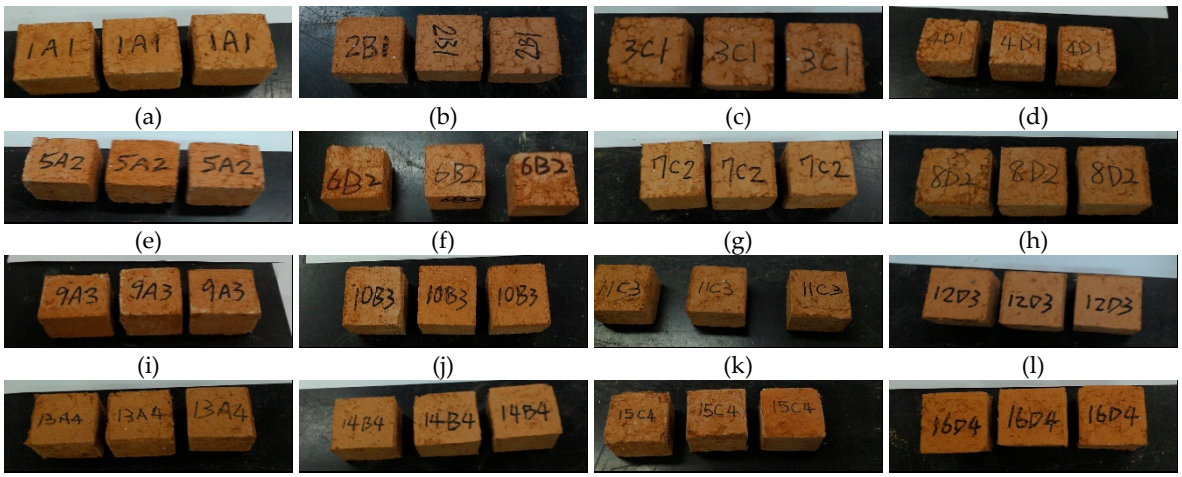

Figure 6. Appearance of fired bricks. (a) G1; (b) G2; (c) G3; (d) G4; (e) G5; (f) G6; (g) G7; (h) G8; (i) G9; (j) G10; (k) G11; (l) G12; (m) G13; (n) G14; (o) G15; (p) G16.

In general, the lighter the brick is, the better it is for transportation and construction. Therefore, the smaller the density, the better. Table 6 shows that the density of the produced brick ranged between 1.57 and 1.84 g/cm^3. Moreover, the lowest value of density was 1.57 g/cm^3 (experiment number G4). Table 7 (i.e., the response table) shows the mean *S*/*N* ratio at each level of the parameters (A–E) for density, while Figure 7 shows the *S*/*N* response graph for density. As shown in Equation (4), the larger the *S*/*N* ratio, the smaller the variance of density around the desired (the-smaller-the-better) value. From Table 7 and Figure 7, it can be seen that the cullet content was the most important factor affecting the responses; the maximum value of response was at the lowest level of the cullet content. In other word, the greater the amount of TFT-LCD waste glass powder added, the higher the density of the resulting bricks. The results of the ANOVA of density are given in Table 8. In addition, the *F* values were obtained for a 95% level of confidence and the percentage contribution of each parameter was also calculated. The sintering temperature was the most significant factor that contributed to the total density of the brick. The main contributions from the parameters were: cullet content (40.97%), preheat time (20.73%), and sintering temperature (17.21%). Thus, based on the results of the *S*/*N* ratio and ANOVA analyses, the optimal combination of parameters and their levels for achieving minimum density is $A_1B_3C_3D_4$, i.e., cullet content at level 1, drying method at level 3, preheat time at level 3, and sintering temperature at level 4.

Table 7. *S*/*N* response table for density.

Parameter	Mean *S*/*N* Ratio (η, Unit: dB)				Delta (Max. η − Min. η)	Rank
	Level 1	Level 2	Level 3	Level 4		
Cullet Content, A (%)	−4.21	−4.61	−4.65	−4.92	0.71	1
Drying Method, B	-4.88	−4.53	−4.45	−4.54	0.43	3
Preheat Time, C (min)	-4.62	−4.71	−4.52	−4.54	0.19	5
Sintering Temperature, D (°C)	−4.52	−4.61	-4.87	-4.40	0.47	2
Error, E	−4.62	−4.41	−4.74	−4.62	0.33	4

Table 8. Analysis of variance and *F* test for density.

Parameter	Sum of Square (SS_Z)	Degree of Freedom	Variance (MS_Z)	*F* Value (F_Z)	$F_{0.05,3,3}$	Percentage Contribution (P_Z)	Note
Cullet Content, A (%)	1.01	3	0.34	10.88	9.28	40.97	Significant
Drying Method, B	0.43	3	0.14	4.61	9.28	14.96	
Preheat Time, C (min)	0.09	3	0.03	1.00	9.28	20.73	
Sintering Temperature, D (°C)	0.48	3	0.16	5.15	9.28	17.21	
Error, E	0.23	3	0.08	2.48	9.28	6.13	
All Other	0.09	3	0.03				
Total	2.24	15	0.75			100	

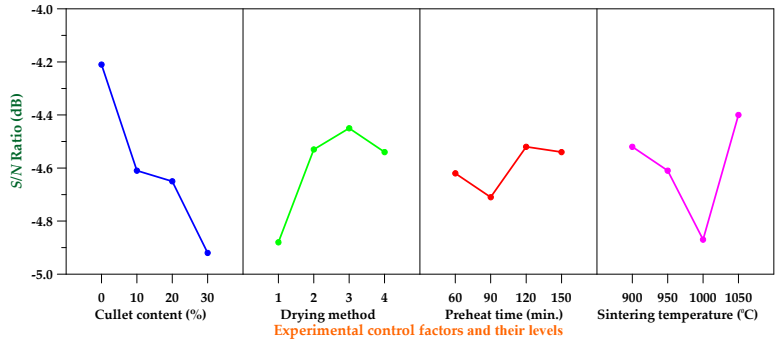

Figure 7. *S/N* response graph for density.

3.3. Water Absorption

It can be seen from Table 6 that the water absorption of the produced brick ranged between 12.5–30.3%. Water absorption is an important indicator of the characteristics of building bricks, and its water absorption should not be too high. This is because the durability of bricks depends to a large extent on their water absorption. Generally speaking, high water absorption of the sintered brick will reduce its service life. According to CNS 382 [32], the water absorption of building bricks requires that the first-class bricks have a water absorption of 15% or less for 24 hours, and a second-class brick has a water absorption of 19% or less for 24 hours. The lowest value of water absorption was around 12.5% and was obtained with Sample G13. Table 9 shows the mean *S/N* ratio at each level of the parameters for water absorption, while Figure 8 shows the *S/N* response graph for water absorption. It is evident from Table 9 and Figure 8 that the cullet content was the most critical factor affecting water absorption; the maximum value of response was at the highest level of cullet content. In addition, the greater the amount of TFT-LCD waste glass powder added, the lower the water absorption of the resulting bricks. The results of the ANOVA of water absorption are given in Table 10. As can be easily seen from Table 10, the cullet content was the most significant factor that contributed to the total water absorption of the brick. In addition, the sintering temperature also affects the water absorption of the bricks. This is because a higher sintering temperature ensures the completion of the crystallization process and closes the open pores in the sinter. The contributions from these parameters were: cullet content (58.57%), sintering temperature (23.93%), drying method (1.77%), and preheat time (0.61%). Therefore, based on the results of the *S/N* ratio and ANOVA analyses, the optimal combination of parameters and their levels for achieving minimum water absorption is $A_4B_4C_2D_3$, i.e., cullet content at level 4, drying method at level 4, preheat time at level 2, and sintering temperature at level 3.

Table 9. *S/N* response table for water absorption.

Parameter	Mean *S/N* Ratio (η, Unit: dB)				Delta (Max. η − Min. η)	Rank
	Level 1	Level 2	Level 3	Level 4		
Cullet Content, A (%)	−28.29	−26.28	−26.36	−23.78	4.51	1
Drying Method, B	−26.19	−26.59	−26.16	−25.77	0.82	4
Preheat Time, C (min)	−26.15	−26.10	−26.16	−26.30	0.20	5
Sintering Temperature, D (°C)	−27.01	−25.57	−24.82	−27.32	2.50	2
Error, E	−26.32	−26.92	−24.81	−26.66	2.11	3

Table 10. Analysis of variance and *F* test for water absorption.

Parameter	Sum of Square (SS_Z)	Degree of Freedom	Variance (MS_Z)	*F* Value (F_Z)	$F_{0.05;3,3}$	Percentage Contribution (P_Z)	Note
Cullet Content, A (%)	41.05	3	13.68	481.07	9.28	58.57	Significant
Drying Method, B	1.32	3	0.44	15.51	9.28	1.77	
Preheat Time, C (min)	0.09	3	0.03	1.00	9.28	0.61	
Sintering Temperature, D (°C)	16.82	3	5.61	197.13	9.28	23.93	Significant
Error, E	10.66	3	3.55	124.94	9.28	15.12	Sub significant
All Other	0.09	3	0.03				
Total	69.94	15	23.31			100.00	

Preprints (www.preprints.org) | NOT PEER-REVIEWED | Posted: 14 June 2018 doi:10.20944/preprints201806.0229.v1

Peer-reviewed version available at Sustainability 2018, 10, 2503; doi:10.3390/su10072503

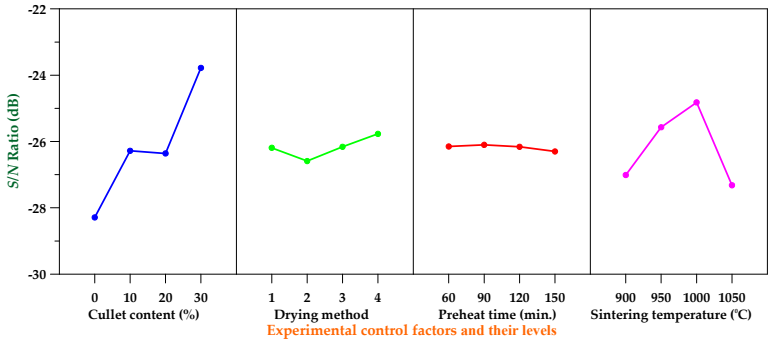

Figure 8. *S/N* response graph for water absorption.

3.4. Shrinkage Ratio

In the firing process, the volume of brick embryo shrank. Table 6 shows that the shrinkage ratio of the produced brick ranged between 12.5 and 47.6%. In other words, the largest value of shrinkage ratio was around 47.6% and was obtained with Sample G5. Table 11 shows the mean *S/N* ratio at each level of the parameters for shrinkage ratio, while Figure 9 shows the *S/N* response graph for shrinkage ratio. From Table 11 and Figure 9, it can be seen that the drying method was the most important factor affecting shrinkage; the maximum value of response was drying method 3. The results of the ANOVA of shrinkage ratio are given in Table 12. The contributions from these parameters were: drying method (48.44%), preheat time (27.63%), and sintering temperature (16.55%). As a result, according to the results of the *S/N* ratio and ANOVA analyses, the optimal combination of parameters and their levels for achieving minimum shrinkage ratio is $A_3B_3C_4D_1$, i.e., cullet content at level 3, drying method at level 3, preheat time at level 4, and sintering temperature at level 1.

Table 11. *S/N* response table for shrinkage ratio.

Parameter	Mean *S/N* Ratio (η, Unit: dB)				Delta (Max. η – Min. η)	Rank
	Level 1	Level 2	Level 3	Level 4		
Cullet Content, A (%)	-28.47	-27.69	-27.20	-28.40	1.27	5
Drying Method, B	-30.89	-27.10	-25.86	-27.90	5.03	1
Preheat Time, C (min)	-28.86	-28.48	-27.74	-26.68	2.18	4
Sintering Temperature, D (°C)	-26.73	-28.17	-29.74	-27.12	3.01	2
Error, E	-27.53	-26.74	-28.98	-28.51	2.24	3

Table 12. Analysis of variance and *F* test for shrinkage ratio.

Parameter	Sum of Square (SS_Z)	Degree of Freedom	Variance (MS_Z)	*F* Value (F_Z)	$F_{0.05,3,3}$	Percentage Contribution (P_Z)	Note
Cullet Content, A (%)	4.44	3	1.48	1.00	9.28	0.00	
Drying Method, B	54.99	3	18.33	12.40	9.28	48.44	Significant
Preheat Time, C (min)	11.08	3	3.69	2.50	9.28	27.63	
Sintering Temperature, D (°C)	21.71	3	7.24	4.89	9.28	16.55	
Error, E	12.14	3	4.05	2.74	9.28	7.38	
All Other	4.44	3	1.48				
Total	104.35	15	34.78			100.00	

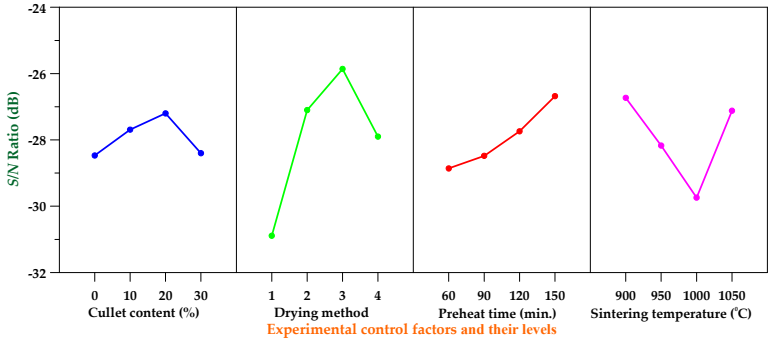

Figure 9. *S/N* response graph for shrinkage ratio.

Preprints (www.preprints.org) | NOT PEER-REVIEWED | Posted: 14 June 2018 doi:10.20944/preprints201806.0229.v1

Peer-reviewed version available at Sustainability 2018, 10, 2503; doi:10.3390/su10072503

3.5. Loss on Ignition

Loss on ignition is the basis for calculation of the balance of energy required for production. From Table 6, it is clear that the loss of ignition of the produced brick ranged between 4.1 and 20.6%. Moreover, the lowest value of loss on ignition was 4.1% and was obtained with Sample G15. Table 13 shows the mean *S/N* ratio for each level of the parameters for loss on ignition, while Figure 10 shows the *S/N* response graph for loss of ignition. From Table 13, it can be seen that the drying method was the most significant factor in controlling ignition loss. The results of the ANOVA of loss on ignition are given in Table 14. The contributions from these parameters were: drying method (97.79%), cullet content (1.28%), preheat time (0.76%), and sintering temperature (0.18%). As a result, according to the results of the *S/N* ratio and ANOVA analyses, the optimal combination of parameters and their levels for achieving minimum loss on ignition is $A_4B_3C_2D_4$, i.e., cullet content at level 4, drying method at level 3, preheat time at level 2, and sintering temperature at level 4.

Table 13. *S/N* response table for loss on ignition.

Parameter	Mean *S/N* Ratio (η, Unit: dB)				Delta (Max. η – Min. η)	Rank
	Level 1	Level 2	Level 3	Level 4		
Cullet Content, A (%)	−20.92	−20.59	−19.76	−19.51	1.41	2
Drying Method, B	−23.89	−25.65	−13.83	−17.41	11.82	1
Preheat Time, C (min)	−20.46	−19.92	−20.20	−20.19	0.54	4
Sintering Temperature, D (°C)	−20.34	−20.10	−20.54	−19.80	0.74	3
Error, E	−19.98	−20.47	−20.25	−20.08	0.49	5

Table 14. Analysis of variance and *F* test for loss on ignition.

Parameter	Sum of Square (SS_Z)	Degree of Freedom	Variance (MS_Z)	*F* Value (F_Z)	$F_{0.05,3,3}$	Percentage Contribution (P_Z)	Note
Cullet Content, A (%)	5.35	3	1.78	9.48	9.28	1.28	Sub significant
Drying Method, B	367.01	3	122.34	650.91	9.28	97.79	Significant
Preheat Time, C (min)	0.59	3	0.20	1.04	9.28	0.76	
Sintering Temperature, D (°C)	1.23	3	0.41	2.19	9.28	0.18	
Error, E	0.56	3	0.19	1.00	9.28	0.00	
All Other	0.56	3	0.19				
Total	374.74	15	124.91			100.00	

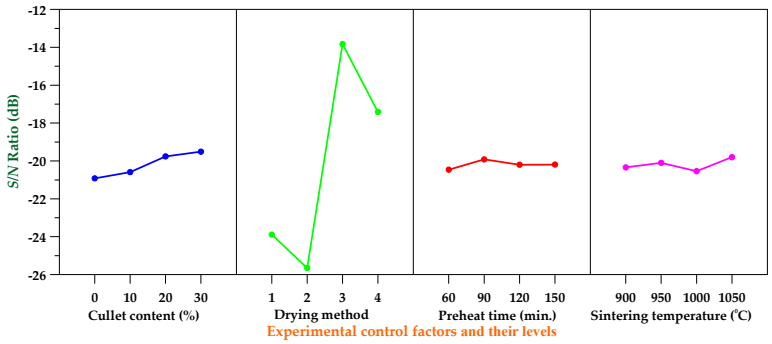

Figure 10. *S/N* response graph for loss on ignition.

3.6. Porosity

Porosity and pore size distribution have long been considered key parameters in determining the durability of bricks. Moreover, the smaller the porosity of the brick, the better the compressive strength. From Table 6, it is clear that the porosity of the produced brick ranged between 20.1 and 42.7%. Moreover, the lowest value of porosity was 20.1% and was obtained with Sample G13. Table 15 shows the mean *S/N* ratio for each level of the parameters for porosity, while Figure 11 shows the *S/N* response graph for porosity. From Table 15, it can be seen that the cullet content was the most significant factor in controlling porosity. The results of the ANOVA of porosity are given in Table 16. The contributions from these parameters were: cullet content (53.16%), sintering temperature (26.57%), drying method (2.48%), and preheat time (1.23%). As a result, according to the results of the *S/N* ratio and ANOVA analyses, the optimal combination of parameters and their levels for achieving

minimum porosity is $A_4B_4C_1D_3$, i.e., cullet content at level 4, drying method at level 4, preheat time at level 1, and sintering temperature at level 3.

Table 15. *S/N* response table for porosity.

Parameter	Mean *S/N* Ratio (η, Unit: dB)				Delta (Max. η – Min. η)	Rank
	Level 1	Level 2	Level 3	Level 4		
Cullet Content, A (%)	−31.68	−30.05	−30.32	−27.85	3.83	1
Drying Method, B	−29.93	−30.43	−29.99	−29.55	0.88	4
Preheat Time, C (min)	−29.90	−29.93	−29.93	−30.13	0.23	5
Sintering Temperature, D (°C)	−30.82	−29.38	−28.69	−31.01	2.32	2
Error, E	−30.18	−30.64	−28.67	−30.42	1.97	3

Table 16. Analysis of variance and *F* test for porosity.

Parameter	Sum of Square (SS_Z)	Degree of Freedom	Variance (MS_Z)	*F* Value (F_Z)	$F_{0.05,3,3}$	Percentage Contribution (P_Z)	Note
Cullet Content, A (%)	30.16	3	10.05	217.13	9.28	53.16	Significant
Drying Method, B	1.54	3	0.51	11.10	9.28	2.48	
Preheat Time, C (min)	0.14	3	0.05	1.00	9.28	1.23	
Sintering Temperature, D (°C)	15.14	3	5.05	109.00	9.28	26.57	Significant
Error, E	9.49	3	3.16	68.32	9.28	16.56	Sub significant
All Other	0.14	3	0.05				
Total	56.48	15	18.83			100.00	

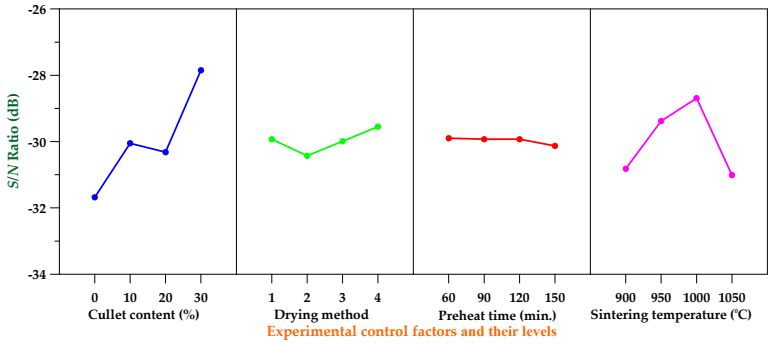

Figure 11. *S/N* response graph for porosity.

3.7. Compressive Strength

The compressive strength of a brick determines its application potential. Its value is usually affected by the porosity, pore size, and type of crystallization. From Table 6, it is clear that the compressive strength of the produced brick ranged between 3.31 and 14.7 MPa. Moreover, the maximum compressive strength was 14.7 MPa and was obtained with Sample G15. Table 17 shows the mean *S/N* ratio for each level of the parameters for compressive strength, while Figure 12 shows the *S/N* response graph for compressive strength. From Table 17, it can be seen that the sintering temperature was the most significant factor in controlling compressive strength. Tay *et al.* [33] pointed out that the clays used to make bricks are low in refractoriness, and vitrification occurs at approximately 1100°C. The resulting viscous bodies reduce porosity and form bonds between the particles, resulting in better strength and hardness of the bricks. The aforementioned phenomenon is generally referred to as porcelainizing. After the brick was porcelainized, it turned from red to grayish black with a glassy phase. From Table 17 and Figure 12, it can be seen that as the sintering temperature increased, the bond between the particles became larger, the pores in the sintered body were reduced, and the compactness was improved, so that the compressive strength of the brick increased. In other words, as the roasting temperature of the brick increased, the compressive strength of the resulting brick increased. In addition, the greater the amount of TFT-LCD waste glass powder, the greater the compressive strength of the brick. The results of the ANOVA of compressive strength are given in Table 18. The contributions from these parameters were: sintering temperature (71.28%), cullet content (17.98%), and preheat time (6.19%). As a result, according to the results of the *S/N* ratio and ANOVA analyses, the optimal combination of parameters and their levels for achieving

maximum compressive strength is $A_3B_1C_3D_4$, i.e., cullet content at level 3, drying method at level 1, preheat time at level 3, and sintering temperature at level 4.

Table 17. *S/N* response table for compressive strength.

Parameter	Mean *S/N* Ratio (η, Unit: dB)				Delta (Max. η – Min. η)	Rank
	Level 1	Level 2	Level 3	Level 4		
Cullet Content, A (%)	13.35	17.26	17.95	17.74	4.60	2
Drying Method, B	17.14	16.54	16.53	16.07	1.07	5
Preheat Time, C (min)	16.99	16.86	17.18	15.26	1.92	4
Sintering Temperature, D (°C)	11.22	15.15	19.41	20.51	9.29	1
Error, E	17.99	16.50	16.64	15.17	2.82	3

Table 18. Analysis of variance and *F* test for compressive strength.

Parameter	Sum of Square (SS_Z)	Degree of Freedom	Variance (MS_Z)	*F* Value (F_Z)	$F_{0.05;3,3}$	Percentage Contribution (P_Z)	Note
Cullet Content, A (%)	56.53	3	18.84	24.36	9.28	17.98	Significant
Drying Method, B	2.32	3	0.77	1.00	9.28	0.00	
Preheat Time, C (min)	9.38	3	3.13	4.04	9.28	6.19	
Sintering Temperature, D (°C)	217.24	3	72.41	93.61	9.28	71.28	Significant
Error, E	16.03	3	5.34	6.91	9.28	4.55	
All Other	2.32	3	0.77				
Total	301.50	15	100.50			100.00	

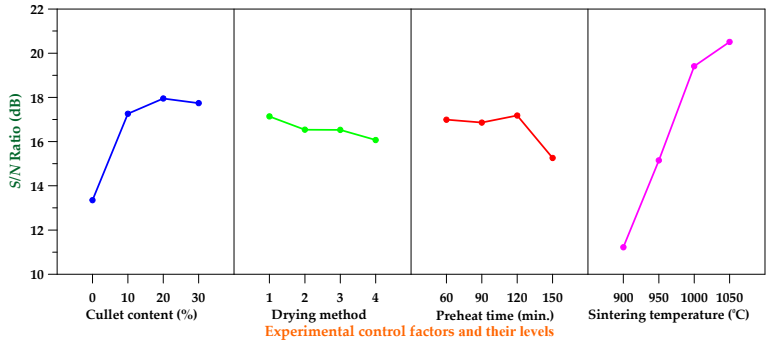

Figure 12. *S/N* response graph for compressive strength.

3.8. Microscopic Analysis of Bricks

Scanning electron microscopy (SEM) was employed to determine the morphology and microstructure of the bricks and capture high resolution digital images. The comparison of SEM images of sintered specimens with pure reservoir sediments (experimental numbers G1-G4) is shown in Figure 13. From Figures 13(a)-(b), it can be seen that when the sintering temperature was between 900 and 950 °C, due to the fact that the temperature required for densification had not yet been reached, the bonding between some powders was not satisfactory. Therefore, the brick specimen was highly porous. In contrast, as can be seen from Figure 13(c), when the sintering temperature was increased to 1000 °C, the powder was provided with a higher neck growth power, resulting in faster interparticle adhesion and distance reduction, and the inside of the brick specimen also showed densification. Further, when the sintering temperature was increased to 1050 °C, the high temperature promotes the diffusion between the particles of the specimen, resulting in a sufficient viscous amorphous glass phase, which can fill the pores between the original particles and gradually cut off the connection between the pores, as shown in Figure 13(d). The fusing together of the clay particles in fired bricks resulted in pore closure which will ultimately lead to reduction in porosity. On the other hand, comparing the SEM images of the specimens with the same waste glass content (experimental numbers G9-G12), it can be seen that the internal compactness of the sintered specimen also had a close relationship with the sintering temperature, as shown in Figure 14. It is clear from Figure 14 that the glassy phase was evenly distributed in the clay body. At 900 °C, the temperature did not reach the sintering point and the interparticle bonding was poor. After sintering at a high temperature (1050 °C), the pores between particles were filled due to diffusion and viscous flow, and

bonds were formed between the particles in the sintered brick, which can increase the degree of densification and further increase the compressive strength of the brick.

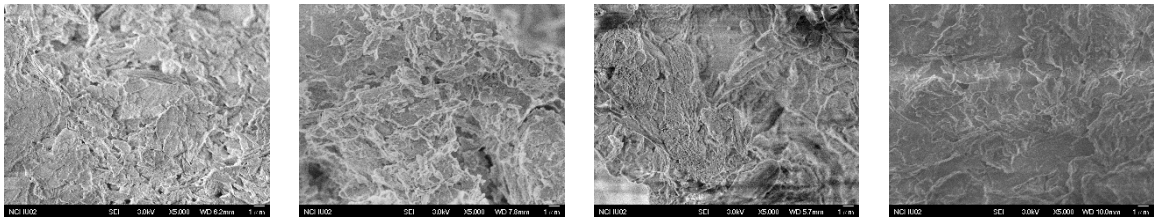

(a) (b) (c) (d)

Figure 13. Comparison of SEM images of sintered specimens with pure reservoir sediments (magnified 5000 times). (a) G1 (sintering temperature 900 °C); (b) G2 (sintering temperature 950 °C); (c) G3 (sintering temperature 1000 °C); and (d) G4 (sintering temperature 1050 °C).

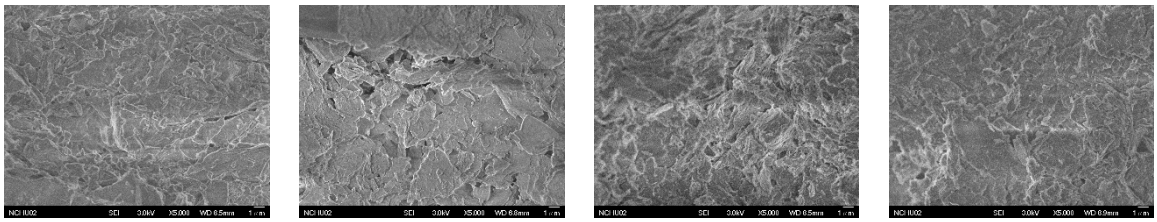

(a) (b) (c) (d)

Figure 14. Comparison of SEM images of sintered specimens with glass and reservoir sediments (magnified 5000 times). (a) G9 (sintering temperature 1050 °C); (b) G10 (sintering temperature 1000 °C); (c) G11 (sintering temperature 950 °C); and (d) G12 (sintering temperature 900 °C).

3.9. Performance of Fired Bricks in Tunnel Kiln

After laboratory-scale brick firing, the best combination was selected based on the pore structure, physical properties, and mechanical properties of the bricks, and a commercial tunnel kiln was used to burn the bricks. The brick-fired tunnel kiln is mainly composed of three parts: preheating, firing, and cooling, as shown in Figure 15. It was a continuous moving ware kiln where the clay products to be fired were passed on trolleys through a long horizontal tunnel. The tunnel kiln is 2 meters high and 2.2 meters wide with a total length of 130 meters. The main focus is on mass production technologies such as raw material processing, brick embryo manufacturing, and firing parameters adjustment (such as sintering temperature, trolley speed, and kiln atmosphere). In addition, the quality of the fired bricks was examined to verify the feasibility of mass production of bricks by incorporating TFT-LCD waste glass powder with reservoir sediments.

(a) (b) (c)

Figure 15. Commercial tunnel kiln. (a) Preheating kiln; (b) Sintering kiln; (c) Cooling kiln.

Regarding the performance requirements of bricks in building construction, more attention is paid to their compressive strength and water absorption. Taking CNS 382 for first-class bricks as an example, the compressive strength should be greater than 14.7 MPa and the water absorption should be less than 15% [32]. According to Table 9 and Table 10, the optimal combination of the lowest obtainable water absorption is estimated to be $A_4B_4C_2D_3$, and according to Table 17 and Table 18, the

optimal combination of the maximum compressive strength is estimated to be $A_3B_1C_3D_4$. In view of this, an experimental combination of fired bricks in the tunnel kiln was proposed. The process conditions are shown in Table 19. Among them, P1 is the optimal combination for producing bricks with the lowest water absorption rate, and P2 is the optimal combination for producing bricks with the highest compressive strength.

Table 19. Process conditions in tunnel kiln.

Experiment Number	Parameter			
	Cullet Content, A (%)	Drying Method, B	Preheat Time, C (min)	Sintering Temperature, D (°C)
P1	30	DM4	90	1000
P2	20	DM1	120	1050

The test results of the fired bricks in the tunnel kiln are shown in Figure 16 and Table 20. From Table 20, it can be seen that the water absorption and compressive strength of the two finished bricks met the requirements of CNS 382 [32]. Among them, experiment number P1 can obtain lower water absorption rate (12.9%); experiment number P2 can obtain higher compressive strength (48.2 MPa) and larger rupture modulus (0.68 MPa). In addition, the density of the two finished bricks was similar, about 2.2 g/cm^3. Compared with the results of the laboratory-scale test, the fired bricks in the tunnel kiln had a higher density and a smaller water absorption. Basically, the cost of bricks for a brick kiln factory includes clay fees, personnel operation and management fees, fuel fees, and transportation fees. However, the use of TFT-LCD waste glass and reservoir sediments to manufacture bricks does not require material fees, and waste disposal fees (government subsidies) are available. Therefore, at least 40% of the cost of each brick can be reduced. This not only solves the problem of disposal of a large amount of TFT-LCD waste glass and reservoir sediments, but also creates a new turning point for the transformation of the brick-making industry.

(a) (b)

Figure 16. Appearance of fired bricks in the tunnel kiln. (a) Experiment Number P1; (b) Experiment Number P2.

Table 20. Test results of fired bricks in tunnel kiln.

Experiment Number	Finished Brick Features			
	Density (g/cm^3)	Water Absorption (%)	Compressive Strength (MPa)	Rupture Modulus (MPa)
P1	2.21	12.9	35.2	0.62
P2	2.24	14.5	48.2	0.68

4. Conclusions

This study presented an application of the Taguchi optimization technique in determining the process condition for producing bricks by incorporating TFT-LCD waste glass powder with reservoir sediments. Experimental results show that by combining TFT-LCD waste glass powders with reservoir deposits, it is possible to produce bricks that comply with CNS standards. Based on the above results and discussion, the following conclusions were drawn:

1. The fired bricks in laboratory-scale had densities ranging between 1.57 and 1.84 g/cm^3, water absorption ranging between 12.5 and 30.3%, and compressive strength ranging between 3.31 and 14.7 MPa. These values were comparable to the general requirements of bricks for buildings.
2. TFT-LCD waste glass can be successfully used in brick manufacture incorporated with reservoir sediments. The water absorption and compressive strength of the fired bricks in the tunnel kiln

are in line with the requirements of CNS 382 for first-class bricks (i.e., the compressive strength should be greater than 14.7 MPa and the water absorption should be less than 15%).

3. The Taguchi method provides a simple, systematic, and efficient methodology for optimizing process conditions of bricks by using grinding TFT-LCD cullet and reservoir sediments and it drastically reduces the number of tests.
4. The use of TFT-LCD waste glass and reservoir sediments to manufacture bricks does not require material costs, and in particular, government subsidies are also available in Taiwan. Therefore, the cost per brick can be reduced by at least 40%.

Acknowledgments: The author expresses his gratitude and sincere appreciation to the Ministry of Science and Technology, Taiwan, for financing this research work.

Conflicts of Interest: The author declares no conflict of interest.

References

1. Somayaji, S. *Civil Engineering Materials*; Prentice Hall: Upper Siddle River, NJ, USA, **2001**.
2. Fernandes, F.M.; Lourenço, P.B.; Castro, F.M. Ancient clay bricks: manufacture and properties. *Materials, Technologies and Practice in Historic Heritage Structures* **2010**, 29–48.
3. Shakir, A.A. Mohammed, A.A. Manufacturing of bricks in the past, in the present and in the future: a state of the art review. *Int. J. Adv. Appl. Sci.* **2013**, *2*, 145-156.
4. Harrison, T.W. Full scale operational trials involving the use of recycled glass additions to clay bricks fired through a tunnel kiln. *The Waste & Resources Action Programme* **2005**, ISBN 1-84405-219-2.
5. Smith, A.S. To demonstrate commercial viability of incorporating ground glass in bricks with reduced emissions and energy savings. *WRAP R&D Report GLA2-018* **2004**, ISBN 1-84405-101-3.
6. Smith, A.S. Glass Addition Trials: York Handmade Bricks Co Ltd. *The Waste & Resources Action Programme* **2005**, ISBN 1-84405-203-6.
7. Rahman, M.E.; Ong, P.J.; Nabinejad, O.; Islam, S.; Khandoker, N.A.N.; Pakrashi, V.; Shorowordi, K.M. Utilization of blended waste materials in bricks. *Technologies* **2018**, 6, 20; doi:10.3390/technologies6010020
8. Rahman, M.E.; Boon, A.; Muntohar, A.S.; Tanim, M.N.H.; Pakrashi, V. Performance of bricks incorporating palm oil fuel ash. *J. Clean. Prod.* **2014**, 78, 195–201.
9. Muntohar, A.S.; Rahman, M.E. Lightweight masonry block from oil palm kernel shell. *Constr. Build. Mater.* **2014**, 54, 477–484.
10. Ean, L.W.; Marlinda, A.M.; Bashar, S.M; Tang, C.W.; Muhammad, T.T. Experimental study on compressive strength of sediment brick masonry. *AIP Conference Proceedings* **2018**, 1930, 020017; doi: 10.1063/1.5022911
11. Kirby, R. Potential energy savings from the use of recycled glass in brick manufacturing, *Center for Environmental Economic Development* **2006**.
12. British Standards Institute. PAS 102. Specification for processed glass for selected secondary end markets **2004**, ISBN 0-580-42588-1.
13. Bernd, W.; Carl, F.S. Utilization of sewage sludge ash in the brick and tile industry. *Water Science and Technology* **1997**, *36*, 251–258.
14. Nagaharu, O.; Shiro, T. Full scale application of manufacturing bricks from sewage. *Wat. Sci. Tech.* **1997**, 36, 243–250.
15. Leshina, V.A.; Pivnev, A.L. Ceramic wall material using glass waste. *Glass and Ceramics* **2002**, *59*, 356–358.
16. Safiuddin, Md.; Jumaat, M.Z.; Salam, M.A.; Islam, M.S.; Hashim, R. Utilization of solid wastes in construction materials. *International Journal of the Physical Sciences* **2010**, *5*, 1952–1963.
17. Demir, I. Reuse of waste glass in building brick production. Waste Manage. Res. 2009, *27*, 572–577.
18. Algin, H.M.; Turgut, P. Cotton and limestone powder wastes as brick material. *Constr. Build. Mater.* **2008**, *22*, 1074–1080.
19. Chidiac, S.E.; Federico, L.M. Effects of waste glass additions on the properties and durability of fired clay brick. *Canadian J. Civil Eng.* **2007**, *34*, 1458–1466.
20. Dondi, M.; Guarini, G.; Raimondo, M.; Zanelli, C. Recycling of PC and TV glass in clay bricks and roof tiles. *Waste Manage* **2009**, *29*, 1945–1951.
21. Lin, K.L. The effect of heating temperature of thin film transistor-liquid crystal display (TFT-LCD) optical waste glass as a partial substitute partial for clay in eco-brick. *Journal of Cleaner Production* **2007**, *15*, 1755–1759.

22. Dalkılıçn, N.; Nabikoğlu, A. Traditional manufacturing of clay brick used in the historical buildings of Diyarbakir (Turkey). *Frontiers of Architectural Research* **2017**, *6*, 346–359.
23. Hegazy, B.E.D.E.; Fouad, H.A.; Hassanain, A.M. Incorporation of water sludge, silica fume, and rice husk ash in brick making. *Advances in Environmental Research* **2012**, 1, 1, 83–96.
24. Loryuenyong, V.; Panyachai, T.; Kaewsimork, K.; Siritai, C. Effects of recycled glass substitution on the physical and mechanical properties of clay bricks. *Waste Management* **2009**, 29, 2717–2721.
25. Taguchi, G. *Introduction to Quality Engineering: Designing Quality into Products and Processes*; Asian Productivity Organization: Tokyo, Japan, 1987.
26. Roy, R.K. *A primer on the Taguchi method*; Van Nostrand Reinhold: New York, NY, USA, 1990.
27. Roy, R.K. *Design of Experiments Using the Taguchi Approach*; John Wiley & Sons Inc.: New York, NY, USA, 2001.
28. Taguchi, G.; Chowdhury, S.; Wu, Y. *Taguchi's Quality Engineering Handbook*; John Wiley & Sons Inc.: New York, NY, USA, 2005.
29. ASTM C67/C67M-18. *Standard Test Methods for Sampling and Testing Brick and Structural Clay Tile*. ASTM International, West Conshohocken, PA, 2018, www.astm.org
30. Neville, A.M. *Properties of Concrete*; Longman: Harlow, Essex, UK, 1994.
31. Chen, H.J.; Chang, S.N.; Tang, C.W. Application of the Taguchi Method for Optimizing the Process Parameters of Producing Lightweight Aggregates by Incorporating Tile Grinding Sludge with Reservoir Sediments. *Materials* **2017**, 10(11), 1294; doi:10.3390/ma10111294.
32. CNS 382. *Bricks for buildings*; Bureau of Standards, Metrology & Inspection, M.O.E.A., R.O.C.: Taipei, Taiwan, 1978.
33. Tay, J.H.; Goh, A.T.C. Engineering properties of incinerator reside. *Journal of Environmental Engineering* **1991**, 117, 2, 224–235.